Final Draft
of the original manuscript:

Pazini Abatti, G.; Nunes Pires, A.T.; Spinelli, A.; Scharnagl, N.; da Conceicao, T.F.:

Conversion coating on magnesium alloy sheet (AZ31) by vanillic acid treatment: Preparation, characterization and corrosion behavior

In: Journal of Alloys and Compounds 738 (2018) 224 - 232
First published online by Elsevier: December 13, 2017

DOI: 10.1016/j.jallcom.2017.12.115
https://doi.org/10.1016/j.jallcom.2017.12.115

Conversion coating on magnesium alloy sheet (AZ31) by vanillic acid treatment: preparation, characterization and corrosion behavior

Guilherme Pazini Abatti [a,*], Alfredo T. Nunes Pires [a], Almir Spinelli [a], Nico Scharnagl [b], Thiago F. da Conceição [a]

[a] Department of Chemistry, Federal University of Santa Catarina, 88040-970 Florianópolis, SC, Brazil

[b] Helmholtz-Zentrum Geesthacht GmbH, Institute of Materials Research, Magnesium Innovations Centre - MagIC, Max-Planck-Str. 1, D-21502 Geesthacht, Germany

e-mail: guipazini@hotmail.com

Abstract

Herein we report the development and characterization of an eco-friendly protective layer of magnesium vanillate on the surface of a magnesium AZ31 alloy sheet, based on a treatment with 1.0 mmol L^{-1} vanillic acid aqueous solution. The coating composition was investigated by XPS and FTIR, and the corrosion behavior of the treated sheets was verified by potentiodynamic polarization and EIS. The results obtained show that the treatment improves corrosion protection and the adhesion of polymer coatings, being a promising treatment for magnesium alloys.

Keywords: Magnesium alloy; Vanillic acid; Conversion coating

1. Introduction

The development of eco-friendly coatings for magnesium alloys is a growing research field [1–5]. These lightweight and biocompatible materials have potential application in the automobile and aerospace industries, as well as in biomedicine [6–9], but their low corrosion resistance inhibits a widespread application [10]. Conversion coatings prepared using hydrofluoric acid [11–13] and chromium [14] present good protective properties, but these chemicals are toxic and the use of chromium is under legal restrictions. Thus, new eco-friendly coatings have been developed based on natural and non-toxic chemicals, as phytic acid [15–18], calcium phosphate [8,19], cerium salts [20–22], chitosan [23] and others.

An interesting strategy to develop new and greener conversion coatings for magnesium alloys is to treat the alloy with natural organic acids, which form insoluble salts with magnesium. In this context, a potential candidate is 4-hydroxy-3-methoxybenzoic acid ($C_8H_8O_4$), known as vanillic acid, a derivative of vanillin [24], the aldehyde responsible for the vanilla flavor (Fig. 1). This acid may react with magnesium, according to the equation 1, forming magnesium vanillate ($Mg(C_8H_7O_4)_2$), which is likely to be insoluble and protect the metal surface from corrosion.

$$2C_8H_8O_4(aq) + Mg(s) \rightarrow Mg(C_8H_7O_4)_2(s) + H_2(g) \quad (1)$$

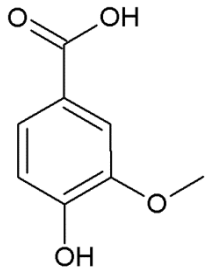

Fig. 1. Chemical structure of the vanillic acid molecule

Besides its natural origin, vanillic acid has analgesic [25], antioxidant [26], antimicrobial [27], and anti-inflammatory properties [28], interesting characteristic for biomedical applications.

Another interesting characteristic of this acid is the presence of hydroxyl and methoxy groups on its chemical structure, which may act as interaction sites for polymer coatings, inducing an adhesion improvement. Thus, the aim of this study was

to prepare and characterize a conversion coating on magnesium AZ31 sheets, by a treatment with vanillic acid, and to evaluate its protective properties in the presence of a corrosive solution. The potential of the prepared coating as a pre-treatment for a polymer coating was also investigated.

2. Experimental

2.1. Materials

Sheets of magnesium alloy AZ31, with dimensions of 5.0 x 2.0 x 0.2 cm, and composition shown below, were used in this study.

Element	Al	Zn	Mn	Si	Cu	Ca	Ni	Fe	Mg
wt.%	2.97	0.85	0.24	0.02	< 0.01	< 0.01	< 0.01	0.03	Bal.

The 4-hydroxy-3-methoxybenzoic acid (vanillic acid) was obtained from Aldrich. NaOH and NaCl were obtained from Vetec. Poly(4-vinylpyridine) (P4VP, M_v = 200,000) was obtained from Scientific Polymer. All chemicals were used without prior purification.

2.2. Conversion coating

The applied conversion coating process consisted of two steps. In the first one, a ground sheet (paper 1200 grid) was immersed in a NaOH 1.0 mol L^{-1} aqueous solution, at room temperature, under mechanical stirring, during 24 h, followed by washing with water. This step forms a magnesium hydroxide layer on the metal surface, which enhances the development of a uniform vanillate layer, as observed in previous studies. Then, it was immersed in a vanillic acid 1.0 mmol L^{-1} aqueous solution at room temperature, under mechanical stirring, for 24 h. Finally, the sheet was washed again with water and dried under vacuum at 100 °C for 24 h. The sheets used in this study are denoted as AZ31A (as-received), AZ31G (ground), AZ31N (NaOH treated) and AZ31V (vanillic acid treated).

2.3. Fourier Transformed Infrared spectroscopy (FTIR)

The infrared spectra of the samples were recorded using the ATR technique in a SHIMADZU IRPrestige-21 spectrophotometer. All measurements were performed in the range of 4000 to 1000 cm^{-1}, in a total of 40 scans with a resolution of 4 cm^{-1}.

2.4. Scanning Electron Microscopy (SEM)

The morphology of the coatings was investigated by means of scanning electron microscopy (SEM), using a Tescan Vega3 SB microscope, operating at 5 kV. Prior to each measurement, the samples were coated with an ultra-thin gold layer.

2.5. X-ray photoelectron spectroscopy (XPS)

X-ray photoelectron spectroscopy (XPS) was performed by using a Kratos DLD Ultra Spectrometer with an Al-Kα X-ray source (monochromator) as anode with power of 225 W. The samples were used as received without any further surface preparation or cleaning. For the survey spectra, a pass-energy (PE) of 160 eV was used while for the region scans PE was 40 eV. Charge neutralization was applied during all measurements. Depth profiling was carried out by using argon ion sputtering with energy of 3.8 keV and a current density of 125 μA cm^{-2}. The etching rate was determined to be 12 nm min^{-1} specific for Ta_2O_5. Data evaluation was done by using CasaXPS Software. The spectra were calibrated to binding energy of 284.5 eV for C-C of the C1s signal. For the depth profiling the region files were quantified without any further deconvolution.

2.6. Corrosion Analyses

Electrochemical Impedance Spectroscopy (EIS) and Potenciodynamic Polarization analyses were performed on a potentiostat PalmSens 3, using a three electrode cell (sample as the working electrode, a graphite rod as auxiliary electrode and Ag/AgCl (KCl saturated) as reference electrode). An area of 1.0 cm^2 was exposed to a NaCl 3.5 wt.% aqueous solution. EIS measurements were performed from 100 kHz to

10 mHz with an amplitude of 10 mV in relation to the open circuit potential (OCP). Two measurements were performed for each sample. Prior to each analysis, the OCP was monitored for 30 min. The potentiodynamic polarization was performed using a scan rate of 0.1 mV s^{-1} from -250 mV to 1000 mV in relation to OCP. A current limit was set at 10 mA for each analysis. These analyses were also performed after 30 min of OCP measurements. Four measurements were performed for each sample.

2.7. Delamination tests

To investigate whether the formed layer could improve the adhesion of polymer coating, poly(4-vinylpyridine) (P4VP) films were prepared on the ground and treated sheets. The P4VP coatings were obtained by casting a P4VP solution in ethanol over the sheets, adjusting the wet thickness using a proper spacer, and letting the solution to dry. Then, a cross-cut was performed on the polymer film and the damaged area was exposed to the solution used in the electrochemical tests. The changes in the aspect of the samples with time were recorded using a digital camera.

3. Results and discussion

3.1. Characterization of the Conversion Coating

The chemical composition of the formed conversion coating was determined by FTIR and XPS analysis. The FTIR spectra for pure vanillic acid, AZ31A, AZ31N and AZ31V are shown in Fig. 2. The signals assignments were performed based on the literature [29–31].

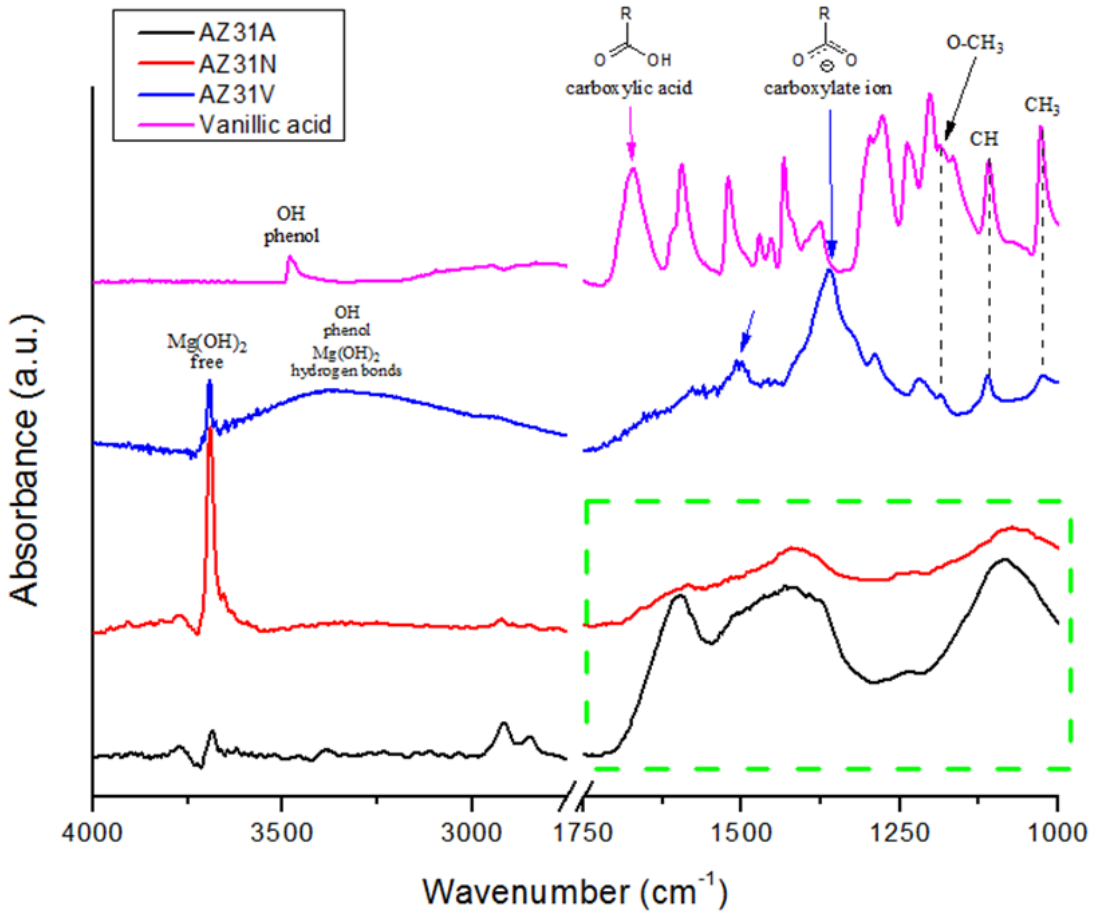

Fig. 2. FTIR spectra for pure vanillic acid, AZ31A, AZ31N and AZ31V.

Characteristic vibrational bands of the carboxylate ion are present in the FTIR spectrum of AZ31V. The two absorption bands are related to the asymmetric (1508 cm^{-1}) and symmetric (1364 cm^{-1}) stretching of the COO^- group, respectively, of magnesium vanillate. Similar bands are described by Swislocka et al. for other alkaline metal vanillates [29]. The C=O vibrational band for vanillic acid (1670 cm^{-1}) does not appear in the spectrum of AZ31V, indicating the conversion of the vanillic acid into a vanillate. The C-C vibrational band (1590 cm^{-1}), related to the aromatic ring, does not appear in AZ31V spectrum due to the convolution caused by the possible mixture of magnesium oxide, magnesium hydroxide and magnesium vanillate on the surface. Nevertheless, the spectra of vanillic acid and AZ31V show similar absorption bands, like the asymmetrical bending of CH_3 group (1024 cm^{-1}), angular deformation of aromatic CH (1108 cm^{-1}) and stretching of O-CH_3 (1185 cm^{-1}). The OH stretching of the phenol group appears as a sharp band on the pure vanillic acid spectrum, at 3481 cm^{-1}, whereas it appears as a broad band, in the range of 2750 cm^{-1} to 3600 cm^{-1}, in the AZ31V

spectrum, which is probably related to hydrogen bonds [29]. In the range of 1750 cm^{-1} to 1000 cm^{-1}, the spectra of AZ31A and AZ31N show convoluted signals related to hydroxides and oxides. The strong and sharp signal at 3693 cm^{-1}, observed on the spectrum of AZ31N is related to the OH stretching of magnesium hydroxide free from hydrogen bonds. It can be observed that this signal is also present in the spectra of AZ31V. These FTIR results suggest a mixture of compounds on top layer of the conversion coating.

To confirm the chemical composition and determine the thickness of the coating, XPS analyses were realized. Fig. 3 shows that the surface composition of the coating is of 51 at.% C, 34 at.% O, and 10 at.% Mg, different from the expected composition for a pure magnesium vanillate layer (41 at.% C, 20 at.% O and 3 at.% Mg), confirming that the surface is comprised of a mixture of magnesium vanillate ($Mg(C_8H_7O_4)_2$), magnesium hydroxide and, possibly, magnesium hydroxy vanillate ($Mg(OH)C_8H_7O_4$). Besides the reaction described in equation 1, the following reactions might take place at the alloy surface during the treatment:

$$Mg(OH)_2(s) + C_8H_8O_4(aq) \rightarrow Mg(OH)C_8H_7O_4(s) + H_2O(l) \quad (2)$$

$$Mg(OH)_2(s) + 2C_8H_8O_4(aq) \rightarrow Mg(C_8H_7O_4)_2(s) + 2H_2O(l) \quad (3)$$

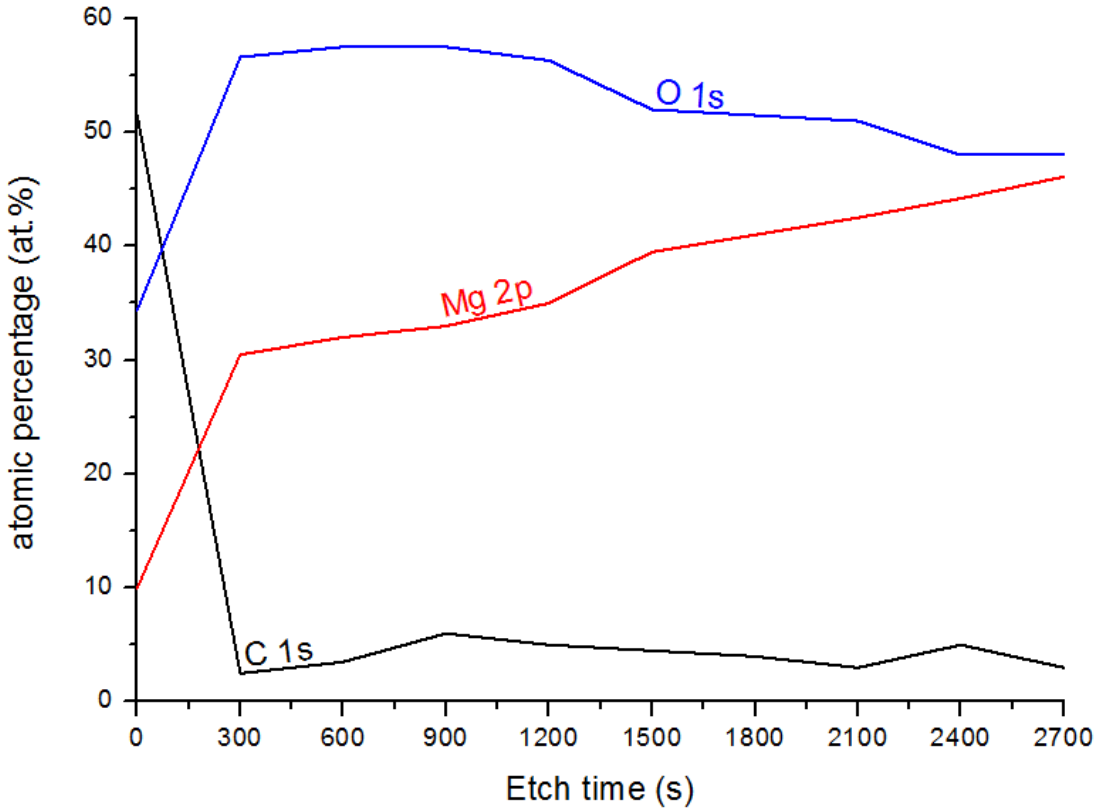

Fig. 3. Depth profile of AZ31V surface, obtained by means of XPS analysis.

The thickness of the conversion coating was estimated based on the concentration of carbon. It can be seen in Fig. 3 that the carbon concentration drops sharply from 51 at.% to about 3 at.% after 300 s of etching, maintaining a constant value therefrom. Considering this residual concentration of carbon as being related to some impurity, and considering the used etching rate of 12 nm min^{-1}, it can be concluded that the vanillate layer has a thickness below 60 nm. It is interesting to observe in Fig. 3 that, when the carbon concentration reaches a minimum, the O/Mg ratio is close to 2, indicating a predominance of magnesium hydroxide beneath the vanillate layer. This ratio goes to 1 as the etching approaches the layer/metal interface, suggesting a region rich in magnesium oxide. Based on these results, it is suggested that the formed layer has the composition shown in Fig. 4.

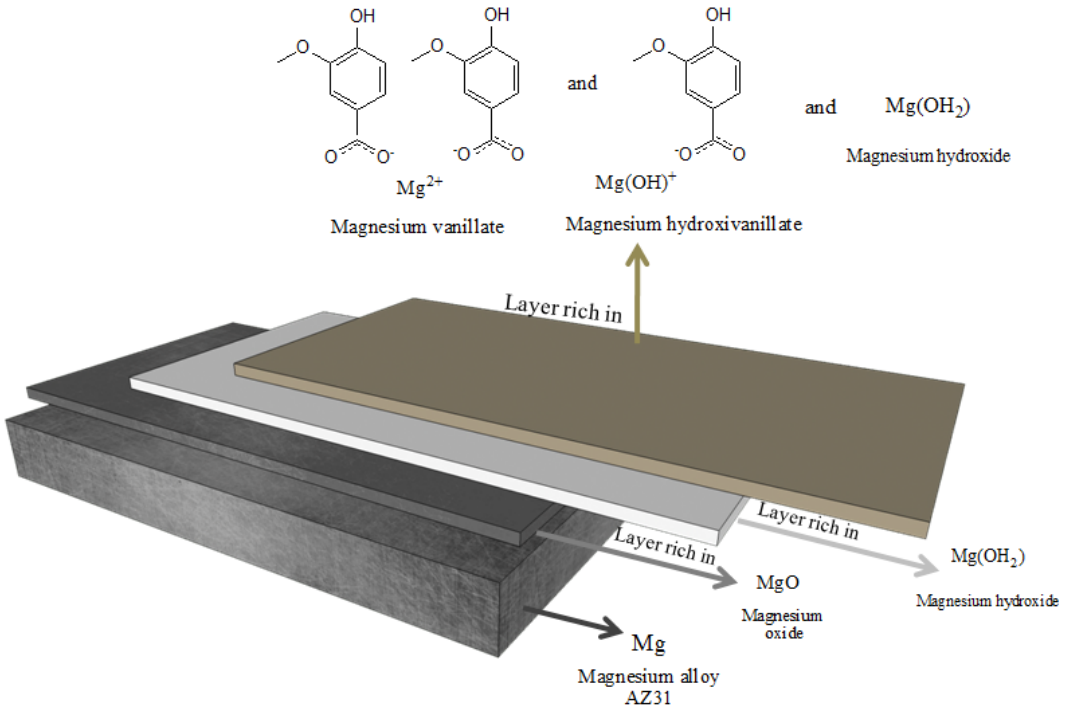

Fig. 4. Schematic representation of the conversion coating composition based on XPS analysis.

Fig. 5 shows the morphology of the conversion coating. It can be seen that the formed coating is compact and that the metal surface is completely covered by it. A higher magnification reveals the presence of some cracks, similar to the observed for other conversion coating processes (inset) [1,15,32].

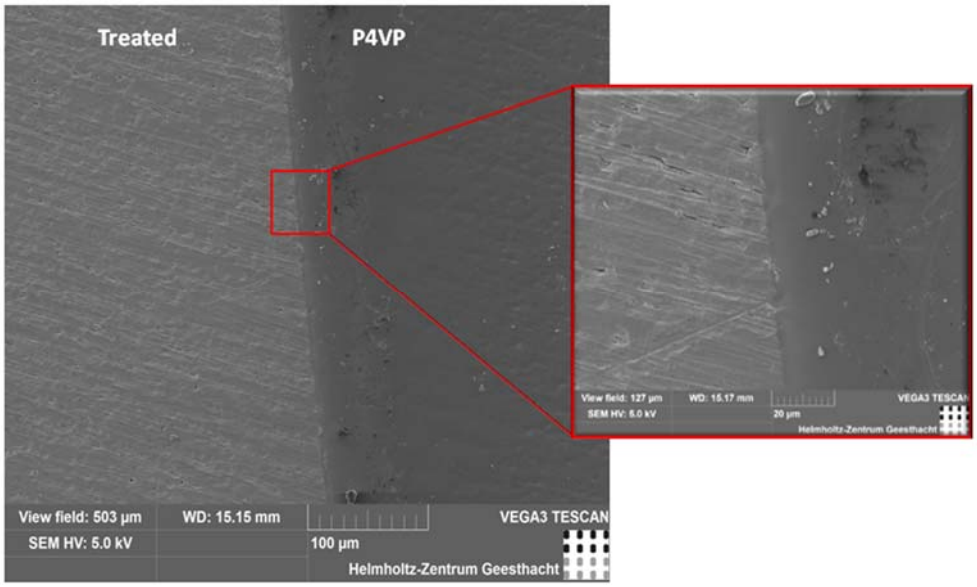

Fig. 5. SEM images of AZ31V. In the inset, a higher magnification of the indicated red square.

3.2. Electrochemical characterization

The results of potentiodynamic polarization are shown in Fig. 6. It can be seen that AZ31V shows a different anodic behavior from AZ31G and AZ31A. Whereas AZ31G and AZ31A show high anodic currents at E_{corr}, AZ31V shows passivation of the metal surface. This indicates that the formed layer has a good adhesion to the metal and provides an effective barrier to the metal dissolution. The cathodic slope (β_c), Table 1, is similar for all samples, indicating that the coating acts as an anodic type inhibitor.

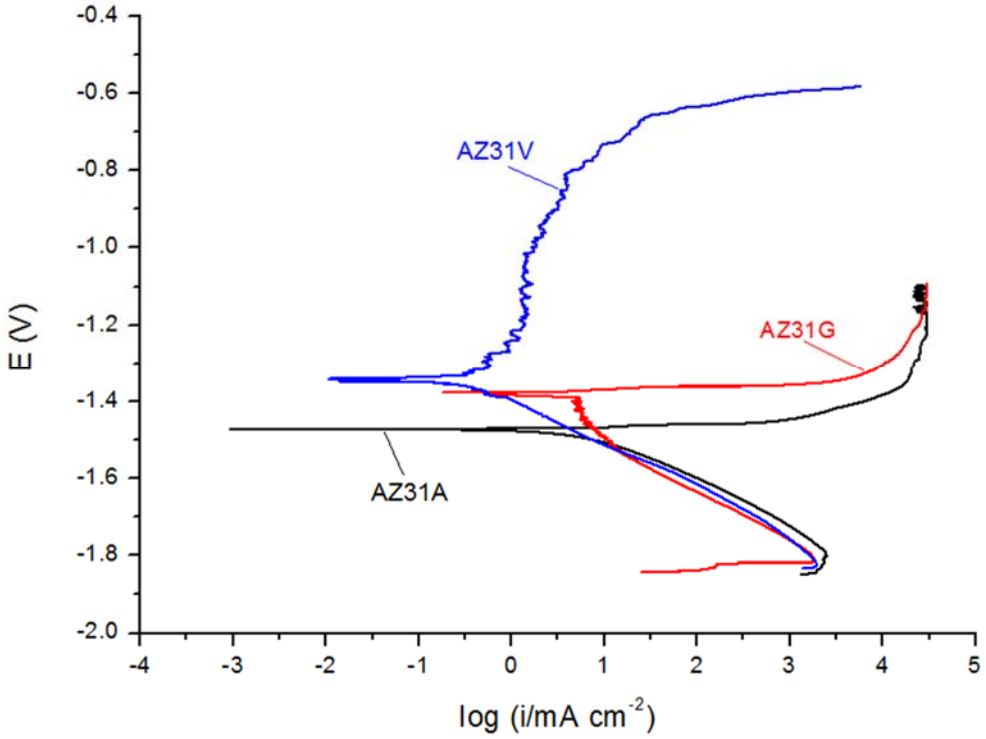

Fig. 6. Potentiodynamic polarization curves of AZ31A, AZ31G and AZ31V.

It can be observed in Table 1 that the grounding process decreases the corrosion current density, what is related to the removal of metallic impurities from the sheet surface, as discussed by Nwaogu [33]. The value of i_{corr} for AZ31G was about thirteen times lower than the observed for AZ31A.

Table 1. Results of potentiodynamic polarization curves for this work and selected references. Four measurements were performed for each AZ31A, AZ31G and AZ31V samples.

Sample	E_{corr} (mV)	i_{corr} (μA cm^{-2})	$-\beta_c$ (mV dec^{-1})	i_{corr} reduction
AZ31A	-1531 ± 6	56.9 ± 21.1	138.31 ± 8.85	
AZ31G	-1512 ± 82	4.27 ± 2.05	128.72 ± 5.04	13
AZ31V	-1352 ± 14	0.58 ± 0.25	144.63 ± 11.78	98
Ce – V [22]*	-1404 ± 80	1.24 ± 0.13	-	82
Cr [18]*	-1468	6.13	-	90
HF [12]*	-1498 ± 23	19.0 ± 10.0	-	6

*In comparison to the i_{corr} value obtained for the as-received sample, for each reference.

A much lower corrosion current is observed for AZ31V, which shows a i_{corr} of almost one hundred times lower than that of AZ31A. Comparing to reports in the literature for Ce, Cr and HF treatments (Table 1), it can be seen that the vanillic acid treatment provides a corrosion protection similar to some of the most used conversion coatings. For an eco-friendly process, this is a remarkable result, especially considering the low thickness of the vanillate layer. For internal comparison, Fig. 7 shows the aspect of the exposed areas of AZ31A, AZ31G and AZ31V after the polarization up to 500 mV above OCP. It can be observed that AZ31A and AZ31G are damaged on the entire exposed area, whereas AZ31V shows only a few spots of corrosion. Even after a polarization up to 1000 mV above OCP, the surface of AZ31V is less damaged.

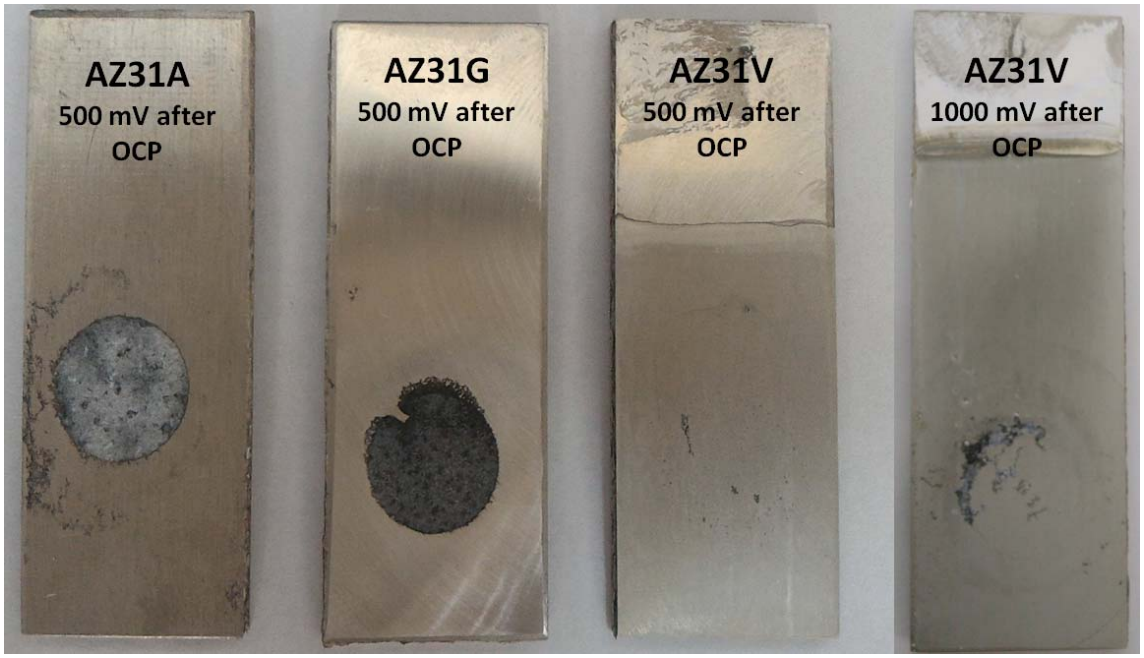

Fig. 7. Aspect of the samples after potentiodynamic polarization tests.

EIS analyses were performed during ten days to obtain a long-term characterization of the coating performance, and the results are shown in Fig. 8. It can be seen that there is a positive influence of mechanical cleaning on the value of the charge transfer resistance (R_{ct}), which was obtained from the diameter of the semicircle. As shown in Table 2, the grounding process increases R_{ct} in approximately two folds, in relation to the as-received sample, at an exposure time of 0.5 h. As discussed for the polarization results, this is related to the removal of metallic impurities.

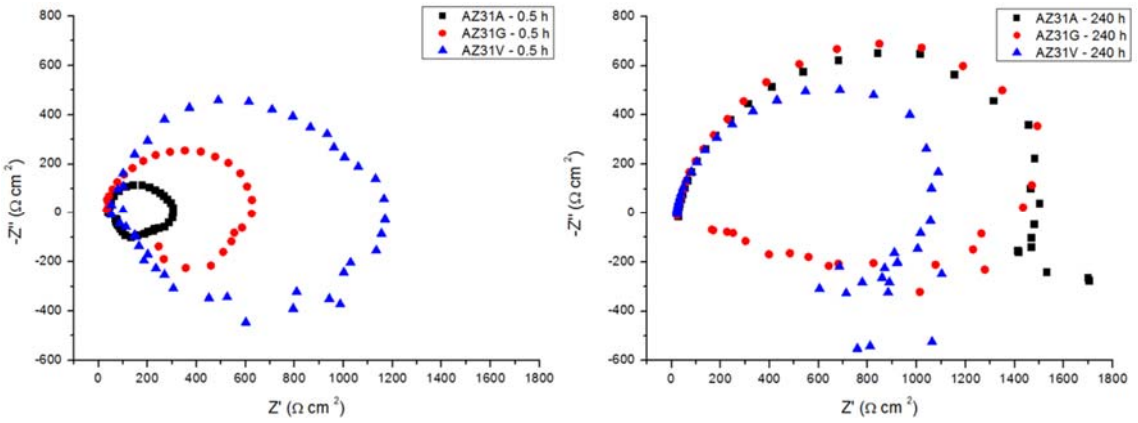

Fig. 8. Nyquist plots of the three samples (A) after 0.5 h and (B) after 240 h of exposure to a 3.5 wt.% NaCl solution.

Table 2. Results obtained from EIS analysis.

Sample	Time (h)	R_{ct} (Ω)*
AZ31A	0.5	270
	240	1,510
AZ31G	0.5	600
	240	1,775
AZ31V	0.5	944
	240	1,060

* Values obtained by the medium value of two samples each.

On the other hand, the treatment with vanillic acid increases R_{ct} in approximately four folds for the same exposure time, a result that confirms the protective nature of the formed coating. After ten days of exposure (240 h), all samples show an increase in the value of R_{ct}, which is related to the deposition of corrosion products on the samples surface, reaching R_{ct} values in the order of 1 kΩ.

3.3. Properties as a pre-treatment for a polymer coating

To evaluate the potential of this process as a pre-treatment for polymer coatings, P4VP coatings were prepared on AZ31G and AZ31V sheets. This polymer was selected due to its interesting properties as a corrosion inhibitor for copper [34], and due to its potential interaction with the hydroxyl group of vanillate [35]. It can be observed in the Bode plot (Fig. 9A) that for AZ31G coated with P4VP, the maximum impedance value (Z_{max}) decreases three orders of magnitude within five days (Table 3), reaching an impedance similar to that of uncoated AZ31G. At this time, it could be observed that the polymer has detached from the substrate.

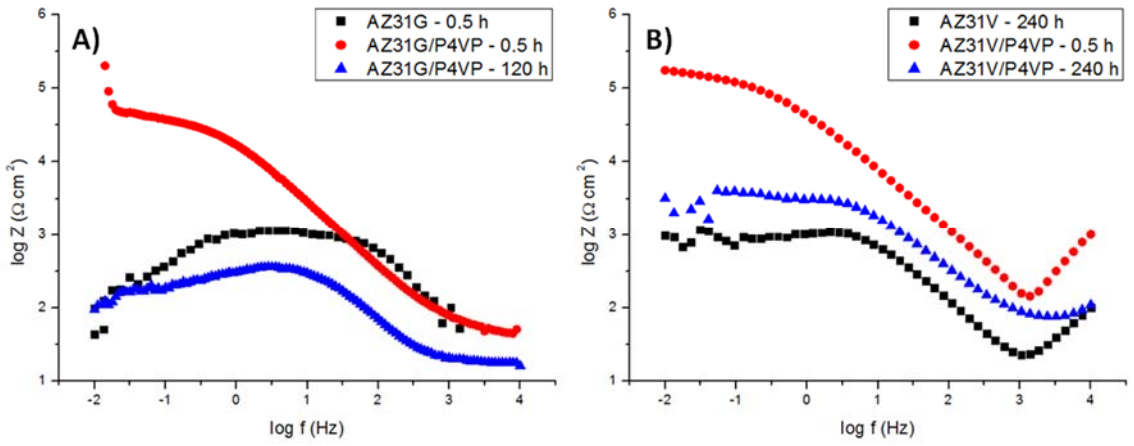

Fig. 9. Bode plot for ground (A) and vanillic acid treated substrates (B), coated with P4VP, in different exposure times to a 3.5 wt.% NaCl solution.

Table 3. Results obtained from EIS analysis.

Sample	Time (h)	Z_{max} (Ω cm^2)*
AZ31G	0.5	653
AZ31G/P4VP	0.5	64,890
	120	684
AZ31V	0.5	960
AZ31V/P4VP	0.5	149,990
	240	3,394

* Values obtained by the medium value of two samples each.

On the other hand, AZ31V coated with P4VP (Fig. 9B) show a much higher Z_{max} value than AZ31V, even after 10 days of exposure. The initial impedance was also higher than the observed for the AZ31G substrate coated with P4VP. Additionally, no film detach was observed during the whole experiment. These results confirm the potential of the vanillic acid treatment as a pre-treatment to improve the performance of polymer coatings. Furthermore, Fig. 10 shows the results of the delamination tests. It can be seen that, after 2 h of exposure to a 3.5 wt. % NaCl solution, the coated AZ31G substrate show signs of corrosion. After 1 day of exposure, the entire exposed area is damaged and after 7 days the metal surface is entirely covered with corrosion product.

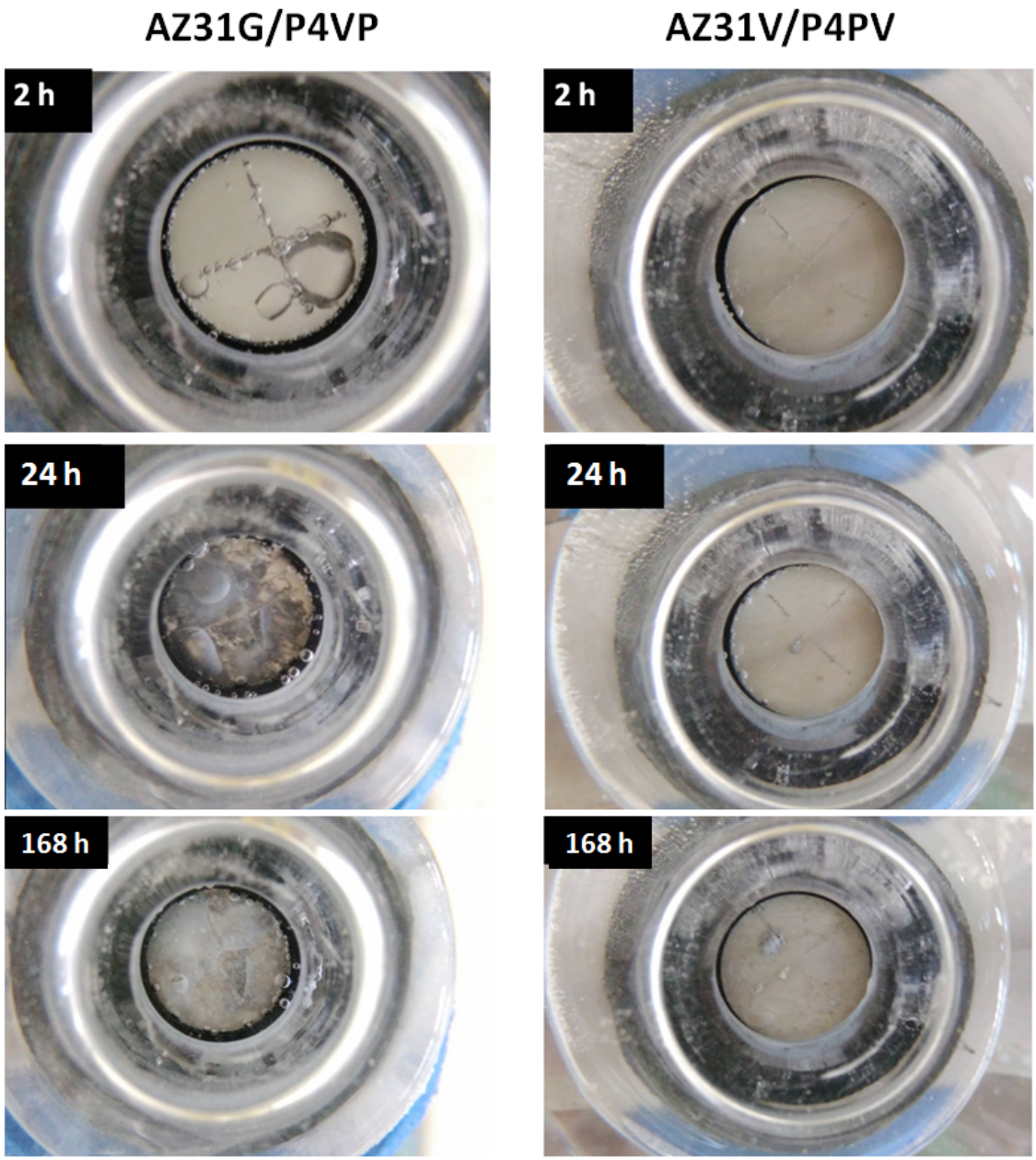

Fig. 10. Aspect of the samples AZ31G/P4VP and AZ31V/P4VP at different times of the delamination test.

For the coated AZ31V substrate, the behavior was different, with only a few corrosion spots on the surface after seven days of exposure. The coating did not detach from the substrate even after 10 days. These results show that the vanillate layer improves the adhesion of the polymer coatings as well as the corrosion protection they offer.

A thinner P4VP coating was prepared on a AZ31V substrate and the sample was analyzed by XPS. Fig. 11 shows the binding energy of the N 1s electron at different

etching times. At the P4VP coating surface, there is a single peak with binding energy of 398.5 eV, attributed to free pyridine groups present in P4VP [35]. At the interface, another peak appears at 399.7 eV that can be attributed to interactions (probably dipole-dipole) of the pyridine ring with functional groups on the vanilate layer [36–38]. The broad band in the range of 401 to 404 eV, indicated by the red rectangle, refers to the hydrogen bonds between the hydroxyl groups present on the vanillate layer and the pyridine groups of P4VP. This result confirms the interaction of the P4VP coating with the vanilate layer. Fig.s 12A and 12B shows schematic representations of the interface of ground and treated samples coated with P4VP.

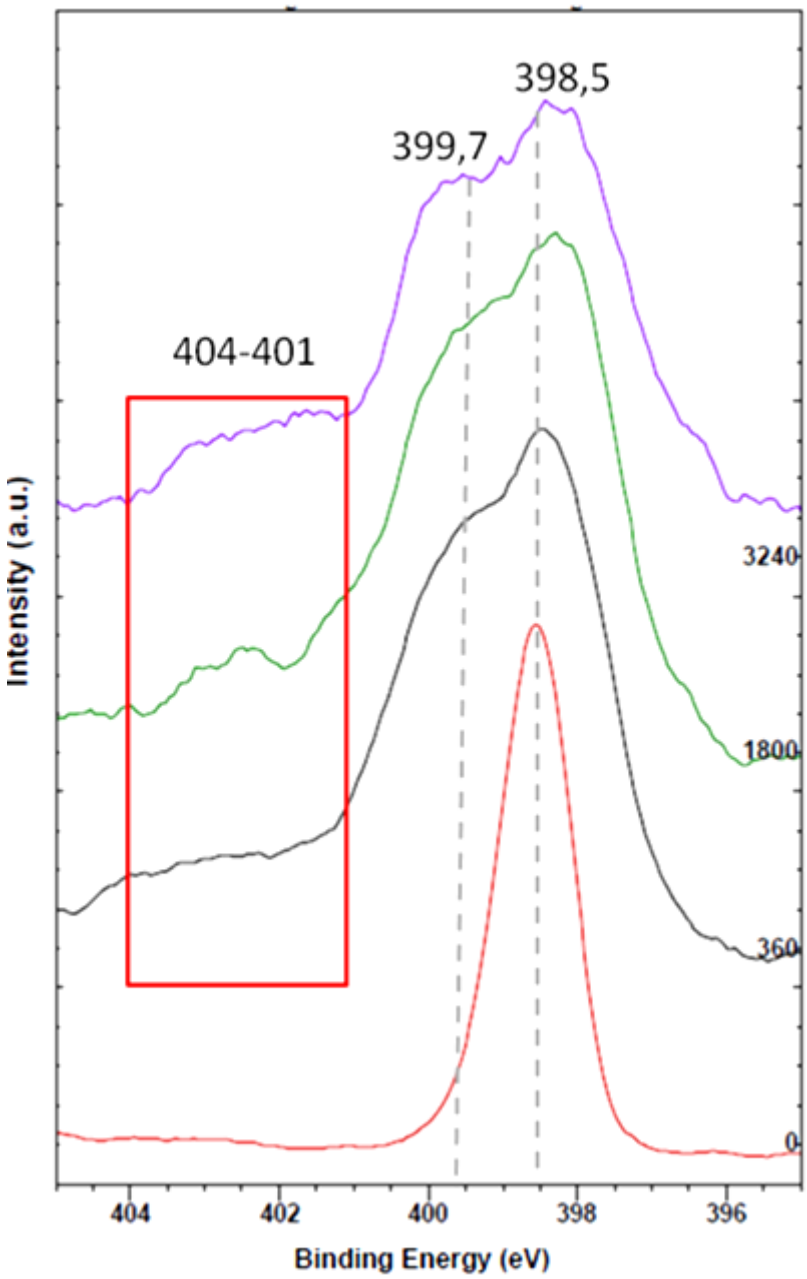

Fig. 11. XPS spectra of the N 1s region for P4VP coated AZ31V with different etching times (0, 360, 1800 e 3240 s).

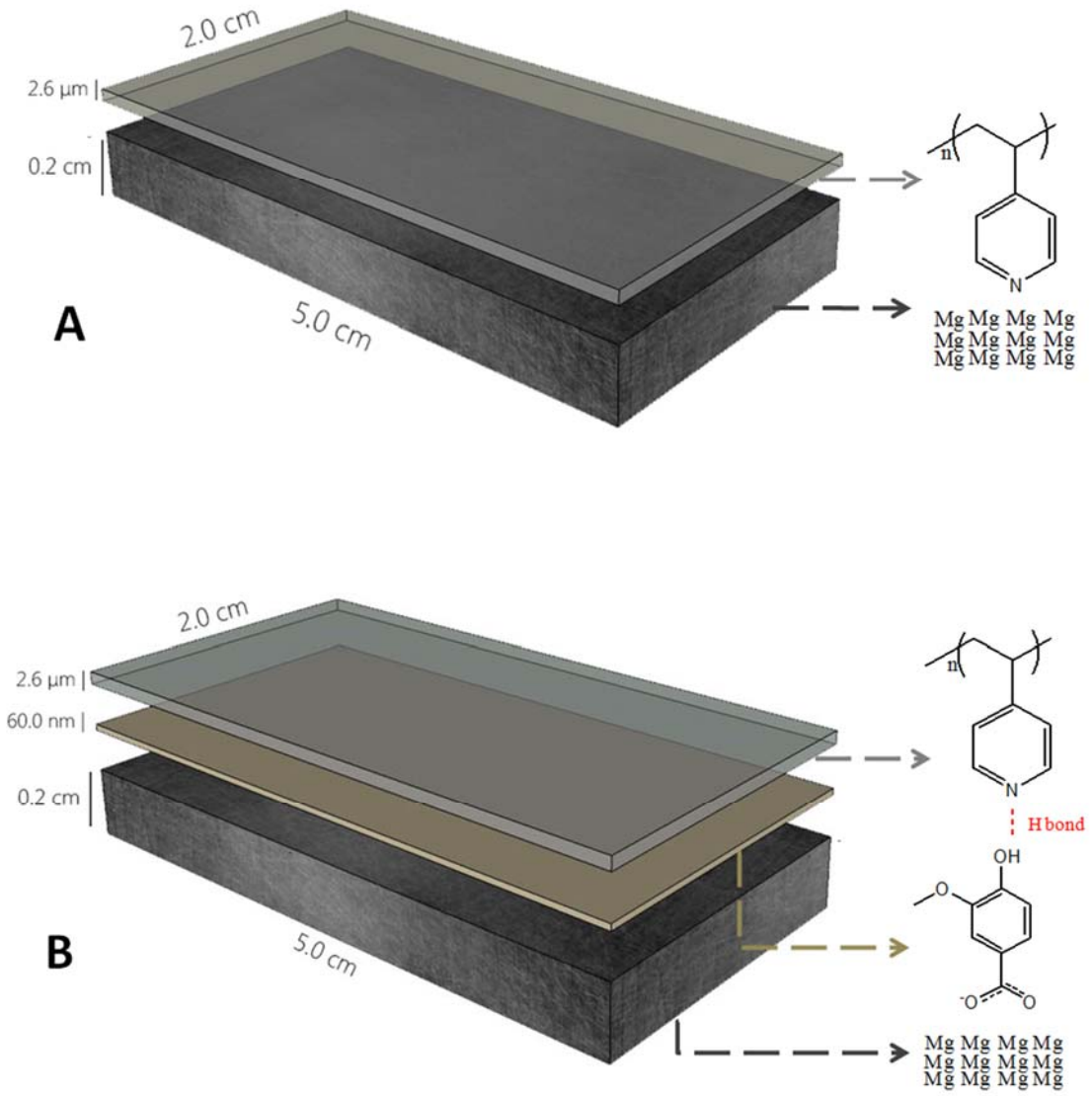

Fig. 12. Schematic representation of the interfacial interaction between P4VP and AZ31G (A) and P4VP and AZ31V (B).

4. Conclusion

The treatment of AZ31 alloy sheets with vanillic acid is an eco-friendly method to form a protective conversion coating on the metal surface. The coating inhibits the anodic dissolution of the metal and reduces the corrosion current in a magnitude similar to the observed for traditional processes described in the literature. As a pre-treatment, the vanillate layer shows the potential to improve the adhesion, and consequently, the protectiveness, of polymer coatings, by means of hydrogen bonds and/or dipole interaction. This is due to the presence of hydroxyl and methoxy groups on its chemical structure. It is a new and promising conversion coating for magnesium alloys.

Acknowledgments

The authors would like to thank CNPq (project number 445263/2014-8) for the financial support of this study.

5. References

[1] Y.R. Chu, C.S. Lin, Citrate gel conversion coating on AZ31 magnesium alloys, Corros. Sci. 87 (2014) 288–296. doi:10.1016/j.corsci.2014.06.034.

[2] Y.L. Lee, Y.R. Chu, W.C. Li, C.S. Lin, Effect of permanganate concentration on the formation and properties of phosphate/permanganate conversion coating on AZ31 magnesium alloy, Corros. Sci. 70 (2013) 74–81. doi:10.1016/j.corsci.2013.01.014.

[3] N.V. Phuong, K.H. Lee, D. Chang, S. Moon, Effects of Zn^{2+} concentration and pH on the zinc phosphate conversion coatings on AZ31 magnesium alloy, Corros. Sci. 74 (2013) 314–322. doi:10.1016/j.corsci.2013.05.005.

[4] S.Y. Jian, Y.R. Chu, C.S. Lin, Permanganate conversion coating on AZ31 magnesium alloys with enhanced corrosion resistance, Corros. Sci. 93 (2015) 301–309. doi:10.1016/j.corsci.2015.01.040.

[5] F. Cao, G.L. Song, A. Atrens, Corrosion and Passivation of Magnesium Alloys, Corros. Sci. 111 (2016) 835–845. doi:10.1016/j.corsci.2016.05.041.

[6] T.A. Grünewald, H. Rennhofer, B. Hesse, M. Burghammer, S.E. Stanzl-Tschegg, M. Cotte, J.F. Löffler, A.M. Weinberg, H.C. Lichtenegger, Magnesium from bioresorbable implants: Distribution and impact on the nano- and mineral structure of bone, Biomaterials. 76 (2016) 250–260. doi:http://dx.doi.org/10.1016/j.biomaterials.2015.10.054.

[7] Q. Chen, G.A. Thouas, Metallic implant biomaterials, Mater. Sci. Eng. R Reports. 87 (2015) 1–57. doi:10.1016/j.mser.2014.10.001.

[8] U. Thormann, V. Alt, L. Heimann, C. Gasquere, C. Heiss, G. Szalay, J. Franke, R. Schnettler, K.S. Lips, The Biocompatibility of Degradable Magnesium Interference Screws: An Experimental Study with Sheep, Biomed. Res. Int. 2015 (2015). doi:10.1155/2015/943603.

[9] E. Willbold, K. Kalla, I. Bartsch, K. Bobe, M. Brauneis, S. Remennik, D. Shechtman, J. Nellesen, W. Tillmann, C. Vogt, F. Witte, Biocompatibility of rapidly solidified magnesium alloy RS66 as a temporary biodegradable metal, Acta Biomater. 9 (2013) 8509–8517. doi:10.1016/j.actbio.2013.02.015.

[10] J.R. Davis, Corrosion: Understanding the basics, first ed., ASM International, Ohio, 2000.

[11] T.F. da Conceição, N. Scharnagl, W. Dietzel, D. Hoeche, K.U. Kainer, Study on the interface of PVDF coatings and HF-treated AZ31 magnesium alloy: Determination of interfacial interactions and reactions with self-healing properties, Corros. Sci. 53 (2011) 712–719. doi:10.1016/j.corsci.2010.11.001.

[12] T.F. da Conceição, N. Scharnagl, C. Blawert, W. Dietzel, K.U. Kainer, Surface modification of magnesium alloy AZ31 by hydrofluoric acid treatment and its effect on the corrosion behaviour, Thin Solid Films. 518 (2010) 5209–5218. doi:10.1016/j.tsf.2010.04.114.

[13] T.F. da Conceição, N. Scharnagl, W. Dietzel, K.U. Kainer, Controlled degradation of a magnesium alloy in simulated body fluid using hydrofluoric acid treatment followed by polyacrylonitrile coating, Corros. Sci. 62 (2012) 83–89. doi:10.1016/j.corsci.2012.04.041.

[14] S. Pommiers, J. Frayret, A. Castetbon, M. Potin-Gautier, Alternative conversion coatings to chromate for the protection of magnesium alloys, Corros. Sci. 84 (2014) 135–146. doi:10.1016/j.corsci.2014.03.021.

[15] R. Zhang, S. Cai, G. Xu, H. Zhao, Y. Li, X. Wang, K. Huang, M. Ren, X. Wu,

Crack self-healing of phytic acid conversion coating on AZ31 magnesium alloy by heat treatment and the corrosion resistance, Appl. Surf. Sci. 313 (2014) 896–904. doi:10.1016/j.apsusc.2014.06.104.
[16] L. Jianrui, G. Yina, H. Weidong, Study on the corrosion resistance of phytic acid conversion coating for magnesium alloys, Surf. Coatings Technol. 201 (2006) 1536–1541. doi:10.1016/j.surfcoat.2006.02.020.
[17] X. Cui, Q. Li, Y. Li, F. Wang, G. Jin, M. Ding, Microstructure and corrosion resistance of phytic acid conversion coatings for magnesium alloy, Appl. Surf. Sci. 255 (2008) 2098–2103. doi:10.1016/j.apsusc.2008.06.199.
[18] H.F. Gao, H.Q. Tan, J. Li, Y.Q. Wang, J.Q. Xun, Synergistic effect of cerium conversion coating and phytic acid conversion coating on AZ31B magnesium alloy, Surf. Coatings Technol. 212 (2012) 32–36. doi:10.1016/j.surfcoat.2012.09.008.
[19] R. Zeng, F. Zhang, Z. Lan, H. Cui, E. Han, Corrosion resistance of calcium-modified zinc phosphate conversion coatings on magnesium-aluminium alloys, Corros. Sci. 88 (2014) 452–459. doi:10.1016/j.corsci.2014.08.007.
[20] L. Lei, X. Wang, W. Liu, Q. Tang, Surface evaluation and electrochemical behavior of cerium conversion coating modified with silane on magnesium alloy, Surf. Interface Anal. 47 (2015) 466–473. doi:10.1002/sia.5734.
[21] X. Cui, Y. Yang, E. Liu, G. Jin, J. Zhong, Q. Li, Corrosion behaviors in physiological solution of cerium conversion coatings on AZ31 magnesium alloy, Appl. Surf. Sci. 257 (2011) 9703–9709. doi:10.1016/j.apsusc.2011.04.141.
[22] X. Jiang, R. Guo, S. Jiang, Microstructure and corrosion resistance of Ce-V conversion coating on AZ31 magnesium alloy, Appl. Surf. Sci. 341 (2015) 166–174. doi:10.1016/j.apsusc.2015.02.195.
[23] L.Y. Pozzo, T.F. da Conceição, A. Spinelli, N. Scharnagl, A.T.N. Pires, Chitosan coatings crosslinked with genipin for corrosion protection of AZ31 magnesium alloy sheets, Carbohydr. Polym. 181 (2018) 71–77. doi:10.1016/j.carbpol.2017.10.055.
[24] F.F. Nord, The formation of lignin and its biochemical degradation, Geochim. et Cosmoch. Acta 28 (1964) 1507-1521.
[25] M. Yrbas, F. Morucci, R. Alonso, S. Gorzalczany, Pharmacological mechanism underlying the antinociceptive activity of vanillic acid, Pharmacol. Biochem. Behav. 132 (2015) 88–95. doi:10.1016/j.pbb.2015.02.016.
[26] S. Kumar, P. Prahalathan, B. Raja, Antihypertensive and antioxidant potential of vanillic acid, a phenolic compound in l-NAME-induced hypertensive rats: a dose-dependence study., Redox Rep. 16 (2011) 208–15. doi:10.1179/1351000211Y.0000000009.
[27] P. Delaquis, K. Stanich, P. Toivonen, Effect of pH on the inhibition of Listeria spp. by vanillin and vanillic acid, J. Food Prot. 68 (2005).
[28] P. Prince, S. Rajakumar, K. Dhanasekar, Protective effects of vanillic acid on electrocardiogram, lipid peroxidation, antioxidants, proinflammatory markers and histopathology in isoproterenol induced cardiotoxic rats, Eur. J. Pharmacol. 668 (2011) 233–240. doi:10.1016/j.ejphar.2011.06.053.
[29] R. Świsłocka, J. Piekut, W. Lewandowski, The relationship between molecular structure and biological activity of alkali metal salts of vanillic acid: Spectroscopic, theoretical and microbiological studies, Spectrochim. Acta - Part A Mol. Biomol. Spectrosc. 100 (2013) 31–40. doi:10.1016/j.saa.2012.01.044.
[30] R. Silverstein, F. Webster, D. Kiemle, Spectrometric Identification of Organic Compounds, seventh ed, Wiley, New York, 2005. doi:10.1016/0022-

2860(76)87024-X.
[31] T.F. da Conceição, N. Scharnagl, C. Blawert, W. Dietzel, K.U. Kainer, Corrosion protection of magnesium alloy AZ31 sheets by spin coating process with poly(ether imide) [PEI], Corros. Sci. 52 (2010) 2066–2079. doi:10.1016/j.corsci.2010.02.027.
[32] J. Chen, Y. Song, D. Shan, E.H. Han, Study of the in situ growth mechanism of Mg-Al hydrotalcite conversion film on AZ31 magnesium alloy, Corros. Sci. 63 (2012) 148–158. doi:10.1016/j.corsci.2012.05.022.
[33] U.C. Nwaogu, C. Blawert, N. Scharnagl, W. Dietzel, K.U. Kainer, Effects of inorganic acid pickling on the corrosion resistance of magnesium alloy AZ31 sheet, Corros. Sci. 51 (2009) 2544–2556. doi:doi:10.1016/j.corsci.2009.06.045.
[34] C. Giacomelli, F.C. Giacomelli, V. Schmidt, A.L. Santana, A. Tiburcio, N. Pires, J.R. Bertolino, A. Spinelli, Protective Effect of Poly (4-Vinylpyridine) Containing Surface Films to the Corrosion of Copper, J. Braz. Chem. Soc. 16 (2005) 9–16.
[35] X. Zhou, S.H. Goh, S.Y. Lee, K.L. Tan, XPS and FTIR studies of interactions in poly (carboxylic acid)/ poly (vinylpyridine), Polymer, 39 (1998) 3631–3640.
[36] M. Camalli, F. Caruso, G. Mattogno, E. Rivarola, Adducts of tin(IV) and organotin(IV) derivatives with 2,2′-azopyridine II. Crystal and molecular structure of $SnMe_2Br_2AZP$ and further mössbauer and photoelectronic spectroscopic studies, In. Chim. Acta. 170 (1990) 225–231. doi:10.1016/S0020-1693(00)80479-X
[37] B.J. Lindberg, J. Hedman, Molecular spectroscopy by means of Esca. 6. Group shifts for N, P and as compounds, Chem. Scr. 7 (1975) 155–166.
[38] R. Van Grieken, A. Markowicz, Handbook of X-Ray Spectrometry, second edition , Marcel Dekker, Inc., New York, 2002.

Figures captions

Fig. 1. Chemical structure of the vanillic acid molecule

Fig. 2. FTIR spectra for pure vanillic acid, AZ31A, AZ31N and AZ31V.

Fig. 3. Depth profile of AZ31V surface, obtained by means of XPS analysis.

Fig. 4. Schematic representation of the conversion coating composition based on XPS analysis.

Fig. 5. SEM images of AZ31V. In the inset, a higher magnification of the indicated red square.

Fig. 6. Potentiodynamic polarization curves of AZ31A, AZ31G and AZ31V.

Fig. 7. Aspect of the samples after potentiodynamic polarization tests.

Fig. 8. Nyquist plots of the three samples (A) after 0.5 h and (B) after ten (10) days of exposure to a 3.5 wt.% NaCl solution.

Fig. 9. Bode plot for ground (A) and vanillic acid treated substrates (B), coated with P4VP, in different exposure times to a 3.5 wt.% NaCl solution.

Fig. 10. Aspect of the samples AZ31G/P4VP and AZ31V/P4VP at different times of the delamination test.

Fig. 11. XPS spectra of the N 1s region for P4VP coated AZ31V with different etching times (0, 360, 1800 e 3240 s).

Fig. 12. Schematic representation of the interfacial interaction between P4VP and AZ31G (A) and P4VP and AZ31V (B).